Monodisperse ZnO Nanodots: Synthesis, Charaterization, and Optoelectronic Properties

Yong Hu,[†] Zhimin Jiang,[†] Chengdong Xu,[†] Ting Mei,*[,†] Jun Guo,[‡] and Tim White[‡]

School of Electrical and Electronic Engineering and School of Materials Science and Engineering, Nanyang Technological University, Singapore 639798, Singapore

Received: April 4, 2007; In Final Form: May 9, 2007

An effective and reliable synthetic route has been developed for the preparation of almost perfectly monodisperse 3 to ∼4 nm ZnO nanocrystals. In addition, a PL peak with a blue-shift of 0.16 eV has been observed in the PL spectrum, showing good size uniformity of the nanodots. The band gap has also been verified in the analysis of $I-V$ characteristics of an ITO/ZnO/SiO_2/Al structure, from which the band alignment of the ZnO nanodots on ITO has been determined. This work demonstrates an efficient synthesis of ZnO nanodots and an easy approach to studying physical properties of nanocrystals that will help the material optimization in device application.

Introduction

Deemed as large artificial atoms, semiconductor nanocrystals (so-called quantum dots) exhibit a tunable density of electronic states, which controls many physical properties that can be widely and easily adjusted by modifying composition, size, and shape.[1] Nanocrystals provide strong quantum confinement of electronic carriers (i.e., electrons and holes) at nanometer scales such that their band gaps and luminescence energies are size- and shape-dependent. These dots have now been widely employed as targeted fluorescent labels for biomedical applications.[2−5]

Because of the size and shape dependence of physical properties, much effort has been focused on the development of new strategies for synthesizing nanocrystals with high monodispersity and high size uniformity in recent years, as these are favorable building blocks for the fabrication of nanodevices and are essential for advanced developments in nanoscience and nanotechnology.[6−8] ZnO, with a bulk band gap of 3.3 eV,[9] is a useful wide band gap material in various applications, such as solar cells, ultraviolet (UV) luminescent devices, and chemical sensors.[10,11] Furthermore, since ZnO is one of the few oxides that shows quantum confinement effects in an experimentally accessible size range (<7 nm), monodisperse ZnO nanocrystals are attracting more and more interest in fundamental research and practical applications.[12,13] Very recently, ZnO nancrystals with various shapes were synthesized using a variety of surfactants, such as trioctylphosohine oxide (TOPO), oleic acid (OA), 1-hexadexylamine (1-HAD), *tert*-butylphosphonic acid (TBPA), and tetradecylphosphonic acid (TDPA).[14−18] However, synthesis is challenging because ZnO nanodots tend to aggregate or undergo Ostwald ripening due to their high surface energy.[19,20]

These obstacles can be overcome by employing liquid−solid solution (LSS) synthesis routes. The LSS strategy is based on controlling the phase transfer and separation process across the liquid, solid, and solution interfaces. It has been demonstrated that by carefully properly tuning the chemical reactions at the interfaces, an extensive group of nanocrystals with tunable sizes and hydrophobic surfaces has been prepared. Previously, the LSS synthesis route was described, in which sodium linoleate was used to prepare monodisperse metal, semiconductor, and rare-earth fluorescing nanocrystals successfully.[21] However, in this study, we employed a highly water-soluble alkali (NaOH) to simplify the LSS synthesis route for ZnO nanocrystals and to make it more stable and controllable.

This approach has allowed the large-scale synthesis of monodisperse ZnO nanocrystals with dimensions of about 3−4 nm, whose photoluminescence (PL) exhibits an obvious blue-shifted peak indicative of good size uniformity. The band gap of ZnO nanodots was obtained from the PL measurement, while the band alignment on indium tin oxide (ITO) was measured by analyzing the $I-V$ characteristics of an ITO/ZnO/SiO_2/Al structure.

Experimental Procedures

All the chemical reagents were purchased from Sigma-Aldrich and used without further purification. The ZnO nanocrystals were synthesized as follows. First, 4 mL of linoleic acid, 0.5 g of NaOH, and 16 mL of ethanol were mixed by stirring at room temperature to form a homogeneous solution. Subsequently, 0.5 g of $ZnCl_2$ was dissolved in 7 mL of deionized water by ultrasonic vibration for 5 min. The mixed solution was obtained by adding them together and maintained at room temperature for a few minutes under stirring. Finally, the mixed reactants were transferred into a 40 mL autoclave, sealed, and heated at 110 °C for 10 h. The system was allowed to cool to room temperature, and the product was collected by centrifugation. The product was washed 3 times with deionized water and absolute ethanol.

The X-ray powder diffraction (XRD) measurement of the sample was performed on a Siemens D5005 X-ray diffractometer with Cu Kα radiation at a scanning rate of 0.06 deg s^{-1}. The TEM and HRTEM images were recorded at 200 keV with a JEM-2100F field−-emission transmission electron microscope (JEOL). The PL spectrum was measured on a Fluorolog-3 spectrofluorimeter, and the $I-V$ curves were characterized using a HP 4155A semiconductor analyzer. The ITO/ZnO/SiO_2/Al structure was fabricated as follows. First, ZnO nanodots were

* Corresponding author. Tel.: 0065-67904387; fax: 0065-67904161; e-mail: ETMei@ntu.edu.sg.
[†] School of Electrical and Electronic Engineering.
[‡] School of Materials Science and Engineering.

10.1021/jp0726384 CCC: $37.00
Published on Web 06/14/2007

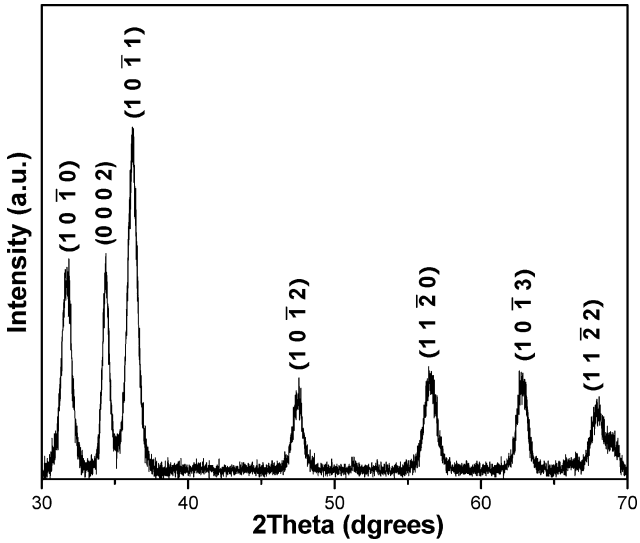

Figure 1. XRD pattern of ZnO nanocrystals.

coated on a layer of 20 nm thickness on the ITO by a spin coating machine at 3000 rpm for 30 s. Then, SiO_2 100 nm in thickness was sputtered on the ZnO nandot layer by a Univex 450B Sputtering System, and the Al electrode was deposited on the SiO_2 layer by a Denton Vacuum DV-502 E-beam system.

Results and Discussion

The composition and phase purity of the as-prepared nanocrystals were established by powder X-ray diffraction (XRD), which confirmed a high degree of crystallinity, with all reflections indexed to wurtzite structured ZnO (JCPDS card no. 89−-0511) with cell parameters $a = 3.249$ Å and $c = 5.205$ Å (in Figure 1). No characteristic peaks of impurities such as $Zn(OH)_2$ were present in detectable quantities.

The corresponding bright field transmission electron microscopy (TEM) image is shown in Figure 2a, and the histogram of the size distribution is given in the inset. This result confirms that the sample consists of nearly monodisperse nanocrystals about 3.5 nm in diameter. Figure 2b is the high-resolution transmission electron micrography (HRTEM) image with fast Fourier transform (FFT) of the ZnO nanodots. It invariably reveals regular lattice spacings, and favorable cases, where the nanocrystal is aligned along a principal axis. The Fourier reconstruction yields a pattern consistent with the wurzite structure.

The PL spectrum of the as-prepared nanodot sample was measured at room temperature with the excitation at a wavelength of 325 nm, as shown in Figure 3. A strong UV light emission peak is clearly observed at 362 nm, corresponding to a transition energy of 3.42 eV. A remarkable blue-shift of 0.16 eV with respect to the edge emission gap energy (3.26 eV) of bulk ZnO crystals[22] is obtained due to the quantum confinement effect in the ZnO nanodots. The corresponding band gap energy is larger than the emission peak energy by the excitonic binding energy. Such an enlarged band gap implies a diameter of 3.5 nm of QDs.[23]

The ZnO nanodots were assembled into an ITO/ZnO/SiO_2/Al structure (in Scheme 1) to further determine the band alignment of ZnO nanodots on ITO via the analysis of $I-V$ characteristics. Figure 4 presents the band diagrams of the ITO/ZnO/SiO_2/Al structure under the two opposite biases. Because of high barriers in both conduction and valence bands at the Al/SiO_2 interface, electron and hole injections from the SiO_2 end were negligible. This is evidenced by the experimental result

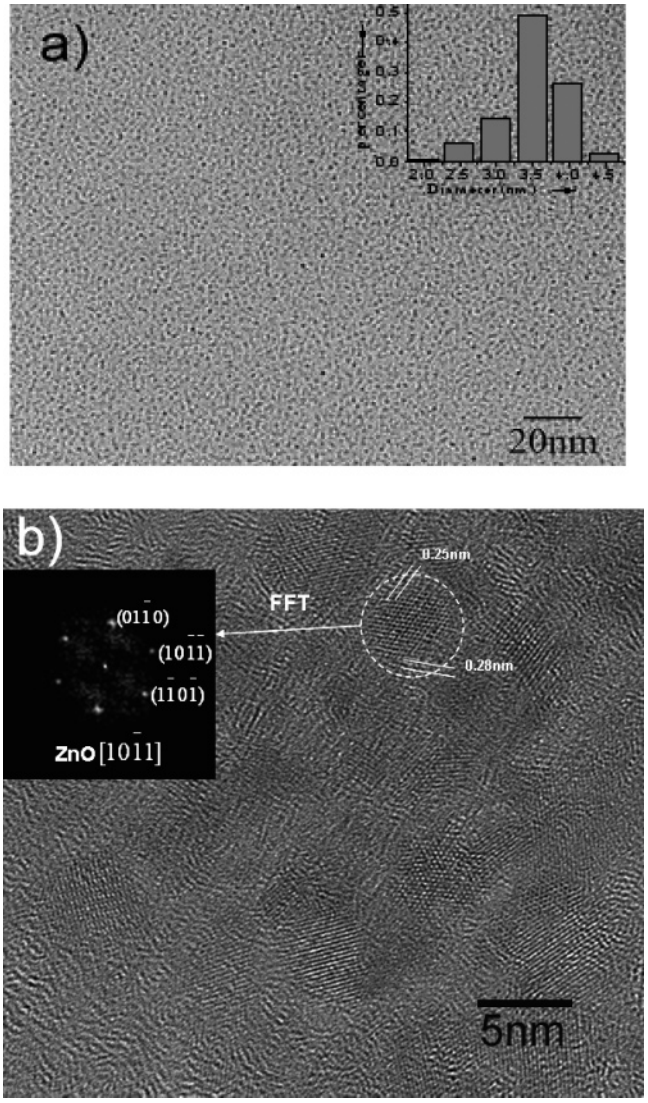

Figure 2. Characterization of monodisperse ZnO nanodots: (a) bright field TEM image and the histogram of the size distribution (inset) and (b) HRTEM image with FFT of the ZnO nanodot.

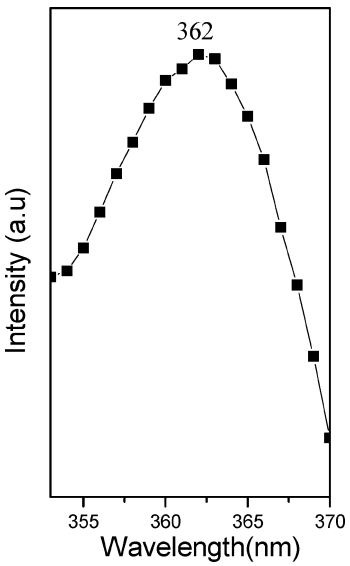

Figure 3. PL spectrum of ZnO nanocrystals ($\lambda_{ex} = 325$ nm).

that the current ratio of ITO/ZnO/SiO_2/Al to ITO/SiO_2/Al is about 100. Figure 5a shows the forward biased $I-V$ character-

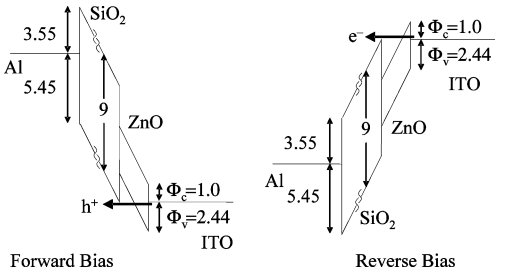

Figure 4. Energy band diagrams for the ITO/ZnO/SiO_2/Al structure biased under a high field showing hole and electron tunneling, respectively.

SCHEME 1 Fabrication of ITO/ZnO/SiO_2/Al Structure

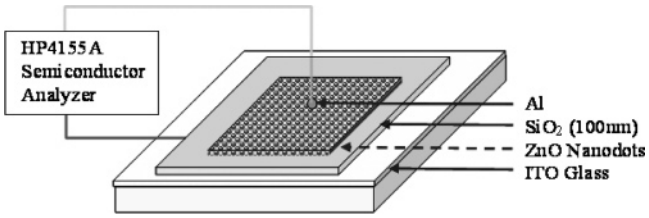

istics of these two structures. Therefore, we can consider unipolar carrier injection in the ITO/ZnO/SiO_2/Al structure. For a sufficiently high bias as illustrated in Figure 4, holes or electrons may tunnel through the ZnO nanodot layer and contribute an appreciable current that follows the Fowler−Nordheim (FN) tunneling equation[24,25]

$$I_{FN} = C_{FN}E^2 \exp\left(-\frac{4}{3}\frac{(2m^*)^{1/2}}{e\hbar}\frac{\phi^{3/2}}{E}\right)$$

where I_{FN} is the current, E is the electric field across the oxide, m^* is the electron or hole effective mass, e is the electronic charge, $\hbar$ is the reduced Planck's constant, and ϕ is the barrier height. As shown in Figure 5b,c, the FN plots $\ln(I/E^2)$ versus $1/E$ at high electric field show a good linearity as a sign of the FN tunneling mechanism. The slopes of -2×10^{10} and -3×10^9 can be determined from the linear regions in forward bias and reverse bias, respectively. Apart from the linear regions, other current injection mechanisms may be dominant (e.g., space charge limited current, etc.). Given effective masses m^*_h ($0.59m_0$) and m^*_e ($0.19m_0$) for hole and electron,[26,27] the barrier heights are calculated to be 2.44 and 1.0 eV, indicating the band alignment of the ZnO nanodots on ITO. The barrier heights sum up to be 3.44 eV, which agrees with the value of the band gap of the ZnO nanodots derived from the PL test very well.

Conclusion

In summary, we have developed an effective and reliable synthetic route for the preparation of almost perfectly monodisperse 3 to ~4 nm ZnO nanocrystals. In addition, a PL peak with a blue-shift of 0.16 eV has been observed in the PL spectrum, showing a good size uniformity of nanocrystals. The band gap has also been verified in the analysis of $I-V$ characteristics of an ITO/ZnO/SiO_2/Al structure, high bias, as holes or electrons may tunnel through the ZnO nanodot layer and contribute an appreciable current that follows the FN tunneling equation, from which the band alignment of the ZnO nanodots on ITO has been determined. This work demonstrates an efficient synthesis of nanodots and an easy approach to studying physical properties of nanocrystals that will help the material optimization in device application.

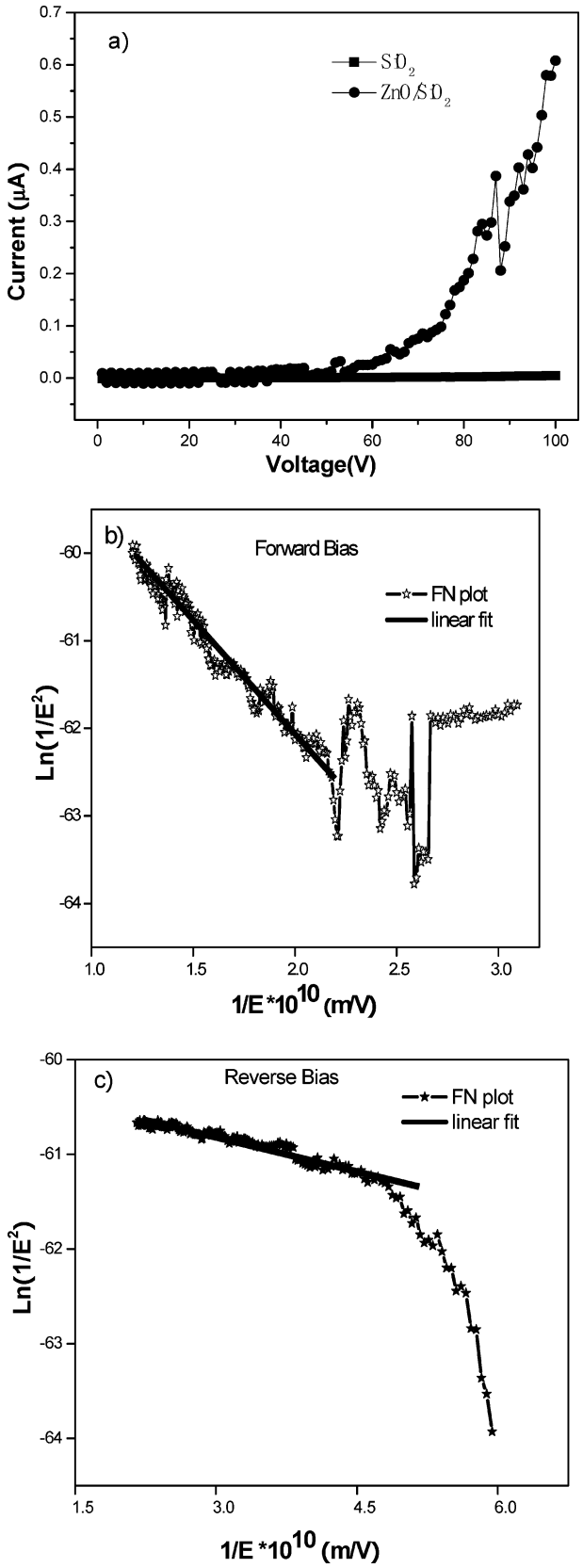

Figure 5. (a) $I-V$ characteristics of the ITO/ZnO/SiO_2/Al and ITO/SiO_2/Al structures at forward bias and −FN plots for the ITO/ZnO/SiO_2/Al structure at (b) forward biases and (c) reverse biases.

Acknowledgment. The authors gratefully acknowledge financial support (Research Grant ARC 2/05) from the Ministry of Education (MOE) and the Agency for Science, Technology and Research (A*STAR), Singapore.

References and Notes

(1) Yin, Y. D.; Alivisatos, A. P. *Nature* **2005**, *437*, 664.
(2) Alivisatos, A. P. *J. Phys. Chem.* **1996**, *100*, 13226.
(3) Bruchez, M.; Moronne, M.; Gin, P.; Weiss, S.; Alivisatos, A. P. *Science* **1998**, *281*, 2013.
(4) Michalet, X.; Pinaud, F. F.; Bentolila, L. A.; Tsay, J. M.; Doose, S.; Li, J. J.; Sundaresan, G.; Wu, A. M.; Gambhir, S. S.; Weiss, S. *Science* **2005**, *307*, 538.
(5) Alivisatos, A. P.; Gu, W.; Larabell, C. *Annu. Rev. Biomed. Eng.* **2005**, *7*, 55.
(6) Sun, S. H.; Murray, C. B.; Weller, D.; Folks, L.; Moser, A. *Science* **2000**, *287*, 1989.
(7) Jin, R.; Cao, Y.; Mirkin, C. A.; Kelly, K. L.; Schatz, G. C.; Zheng, J. G. *Science* **2001**, *294*, 1901.
(8) Sun, Y.; Xia, Y. *Science* **2002**, *298*, 2176.
(9) Viswanatha, R.; Sarma, D. D. *Chem.—Eur. J.* **2006**, *12*, 180.
(10) *Thin Film Solar Cells*; Chopra, K. L., Das, S. R., Eds.; Plenum: New York, 1983.
(11) Hingorani, S.; Pillai, V.; Kumar, P.; Multani, M. S.; Shah, D. O. *Mater. Res. Bull.* **1993**, *28*, 1303.
(12) Radovanovic, P. V.; Norberg, N. S.; McNally, K. E.; Gamelin, D. R. *J. Am. Chem. Soc.* **2002**, *124*, 15192.
(13) Viswanatha, R.; Sapra, S.; Sen Gupta, S.; Satpati, B.; Satyam, P. V.; Dev, B. N.; Sarma, D. D. *J. Phys. Chem. B* **2004**, *108*, 6303.
(14) Joo, J.; Kwon, S. G.; Yu, J. H.; Hyeon, T. *Adv. Mater.* **2005**, *17*, 1873.
(15) Andelman, T.; Gong, Y. Y.; Polking, M.; Yin, M.; Kuskovsky, I.; Neumark, G.; O'Brien, S. *J. Phys. Chem. B* **2005**, *109*, 14314.
(16) Cozzoli, P. D.; Curri, M. L.; Agostiano, A.; Leo, G.; Lomascolo, M. *J. Phys. Chem. B* **2003**, *107*, 4756.
(17) Chen, Y. F.; Kim, M.; Lian, G. D.; Johnson, M. B.; Peng, X. G. *J. Am. Chem. Soc.* **2005**, *127*, 13331.
(18) Choi, S. H.; Kim, E. G.; Park, J. N.; An, K. J.; Lee, N.; Kim, S. C.; Hyeon, T. *J. Phys. Chem. B* **2005**, *109*, 14792.
(19) Ostwald, W. Z. *Phys. Chem.* **1901**, *37*, 385.
(20) Liu, D. P.; Li, G. D.; Su, Y.; Chen, J. S. *Angew. Chem., Int. Ed.* **2006**, *45*, 7370.
(21) Wang, X.; Zhuang, J.; Peng, Q.; Li, Y. D. *Nature* **2005**, *437*, 121.
(22) Wang, L. J.; Giles, N. C. *J. Appl. Phys.* **2003**, *94*, 973.
(23) Lin, K. F.; Cheng, H. M.; Hsu, H. C.; Lin, L. J.; Hsieh, W. F. *Chem. Phys. Lett.* **2005**, *409*, 208.
(24) Zeghbroeck, B. V. *Princ. Semicond. Devices*; **2004**.
(25) Chanana, R. K.; Donald, K. M.; Ventra, M. D.; Pantelides, S. T.; Feldman, L. C.; Chung, G. Y.; Tin, C. C.; Williams, J. R.; Weller, R. A. *Appl. Phys. Lett.* **2000**, *77*, 2560.
(26) Sze, S. M. *Phys. Semicond. Devices* **1981**.
(27) Fan, Z.; Lu, J. G. *J. Nanosci. Nanotechnol.* **2005**, *5*, 1561.